



Starch-templated bio-synthesis of gold nanoflowers for in vitro antimicrobial and anticancer activities

D. Borah¹ · M. Hazarika² · P. Taylor¹ · A. R. Silva³ · B. Chetia² · G. Singaravelu⁴ · P. Das²

Received: 3 July 2017 / Accepted: 23 April 2018 / Published online: 4 May 2018
© Springer-Verlag GmbH Germany, part of Springer Nature 2018

Abstract

We describe an in situ method of synthesizing highly branched gold nanoflower (AuNFs) using aqueous seed extract of *Syzygium cumini* (L.) Skeels as reductant in the presence of 0.3% starch. Surprisingly, when the same reaction was carried out in the absence of starch or with starch at a lower concentration (0.15%), instead of flower-like morphology quasi-spherical or polyhedral nanoparticles (AuNPs) are obtained. The nanomaterials were extensively characterized by HRTEM, FESEM, UV–Vis, FTIR, XRD, XPS and TGA analysis. The biological activities of the materials were investigated for antimicrobial activities against four bacterial strains that include one Gram positive (*Staphylococcus aureus* MTCC 121), two Gram negative (*Escherichia coli* MTCC 40 and *Pseudomonas aeruginosa* MTCC 4673) and one fungi (*Candida albicans* MTCC 227). The nanoparticles functioned as effective antimicrobial and anti-biofilm agents against all the strains under study. Controlled study revealed that, the AuNFs showed improved efficacy over conventional polyhedral AuNPs against all the microbes under study which might be attributed to the larger surface-to-volume ratio of the nanoflowers. The AuNFs also showed effective in vitro anticancer activity against a human liver cancer cell line (HepG2) with no significant cytotoxicity. Our data suggest that the AuNFs can significantly reduce the cancer cell growth with IC₅₀ value of 20 µg mL⁻¹.

Keywords Gold nanoparticles · Nanoflower · Antimicrobial activity · Anticancer activity · Liver cancer

Introduction

Over the past few decades, noble metal nanoparticles have received unprecedented attentions because of their potential utility in various fields such as catalysis, material sciences, heavy metals removal, pharmaceutical sciences, and

biomedical applications (Astruc 2007; Costa and Rossi 2012; Dauthal and Mukhopadhyay 2016). Among various noble metals, gold-based systems are particularly promising for their applicability in the biological domains (Yang et al. 2015; Ackerson et al. 2006; Giljohann et al. 2010), such as photocatalysis (Misra et al. 2017), sensing (Singh et al. 2011), and memory devices (Gupta et al. 2012). Gold, although inert as a bulk metal, in nm scale (particle size 1–100 nm) it is found to be extremely reactive and often shows some unique physical and chemical features that are usually absent in its bulk counterpart. Thus, over the years, synthesis of Au nanoparticles (AuNPs) has drawn many attentions amongst scientific community. It is now established that the properties of metal nanoparticles, especially in biomedical applications, largely depend on their sizes, shapes, morphologies and aggregation patterns (Langille et al. 2012; Personick and Mirkin 2013). Thus, rational design of AuNPs with controlled shape and morphology has become a major field of research (Liu et al. 2012; Grzelczak et al. 2008). Among various methods of synthesizing shape-selective Au nanoparticles, the most popular one is the chemical reduction of Au(III) ion with conventional

D. Borah and M. Hazarika authors contributed equally.

Electronic supplementary material The online version of this article (<https://doi.org/10.1007/s13204-018-0793-x>) contains supplementary material, which is available to authorized users.

✉ P. Das
pankajd29@yahoo.com

- ¹ Centre for Biotechnology and Bioinformatics, Dibrugarh University, Dibrugarh, Assam, India
- ² Department of Chemistry, Dibrugarh University, Dibrugarh, Assam, India
- ³ Aveiro Institute of Materials, University of Aveiro, Aveiro, Portugal
- ⁴ Department of Zoology, Thiruvalluvar University, Vellore, India

reducing agents such as sodium borohydride, hydrogen peroxide, and organic molecules in the presence of some surfactant- or ligand-based stabilizing agents (Dauthal and Mukhopadhyay 2016; Yang et al. 2015; Liu et al. 2012; Zhu et al. 2008; Jana et al. 2001; Sharma and; Chattopodhyay 2004; Bakr et al. 2006; Soetan et al. 2016).

Although the sizes and shapes of such chemically synthesized NPs could be conveniently tuned by controlling reaction parameters such as concentration of gold chloride solution, temperatures, and choice of stabilizers, however, these conventional chemical-based methods are not usually favorable in biological applications. The undesirable toxic substances that are used as reducing or stabilizing agents during the synthesis of nanoparticles often increase the threshold limit of cytotoxicity of such nanoparticles which put serious limitations to their in vivo applications. As a result, during the past few years, efforts are being made to synthesize AuNPs in a more sustainable way using various kinds of biomolecular extracts viz. leaf extract of *Magnolia kobus* (Li et al. 2012), *Centella asiatica* (Das et al. 2010), seed extract of *Abelmoschus Esculentus* (Jayaseelan et al. 2013), *Syzium cumini* (Das et al. 2017), flower extract of *Plumeria alba* (Mata et al. 2016), etc. as potential source of reductant, with or without the assistance of some naturally occurring stabilizers such as cellulose, carbohydrate polymers such as chitosan, starch, and DNA (Liu et al. 2012; Siddiqi and Husen 2017; Opris et al. 2017; Phukan et al. 2016; Virkutyte and Varma 2011; Tiwari et al. 2011; Schreiber et al. 2016; Wang et al. 2010). These bio-inspired stabilizers not only protect the NPs against aggregation but also sometimes act as soft template to attach smaller particles onto its surface in a particular fashion, forming highly branched flower-like structures (Wang et al. 2010). It is noteworthy to mention that branched nanoflowers because of the presence of high surface-to-volume ratio often show successful activities both in the field of catalysis (Ye et al. 2016; Xiao and Qi 2011; Mohanty et al. 2010; Mao et al. 2014) and medicinal biochemistry (Zhao et al. 2009; Xie et al. 2008). Literature survey reveals that the synthesis of gold nanoflowers is mostly limited with chemical-based methods and the plant-based synthesis of gold nanoflower has been rarely reported. Only recently, Ahn et al. 2017 reported synthesis of gold nanoflower using an extract of *Acanthopanax cortex* and successfully investigated their anti-inflammatory activity.

Herein, we report a biogenic method of synthesizing flower-like Au nanoparticles using starch as template with aqueous seed extract of *Syzygium cumini* as reducing agent and investigated their antimicrobial activities against four bacterial strains and anticancer activity against a human liver cancer cell line (HepG2). In addition, the nanomaterials were extensively characterized by techniques such as HRTEM, FESEM, UV–Vis, FTIR, XRD, XPS and TGA analysis. It needs to be mentioned that this particular plant

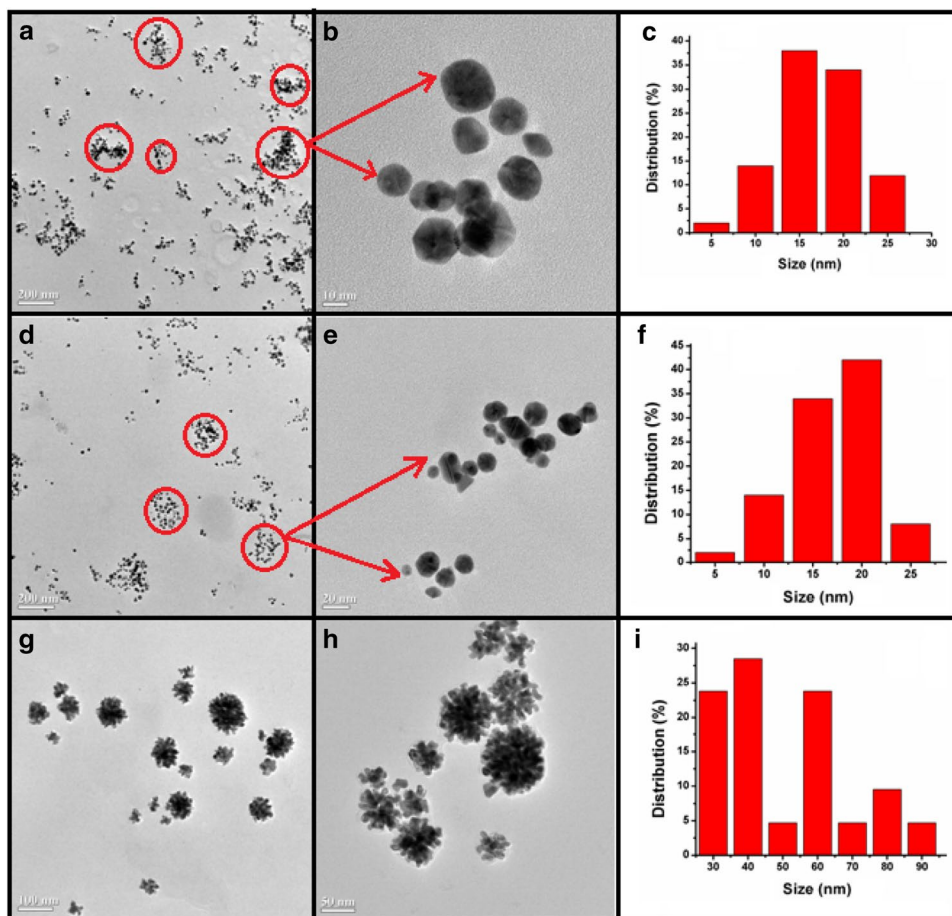
is biologically very important and is usually found in the Indian sub-continent region. In the past decades, the plant has got many scientific attentions because of its utility in various health-beneficial effects such as antidiabetic, anticancer, and antioxidant activities (Liu et al. 2017). The seed of the plant is enriched in flavonoids and polyphenolic compounds such as tannin and gallic acid that have already proven to act as reducing agents for various metal NP synthesis including gold (Das et al. 2017; Swami et al. 2012; Kumar and Yadav 2012). It is also very much pertinent to mention that during the past few years, starch has been receiving immense importance as stabilizing material for shape-selective synthesis of gold nanoparticles because of its low cost, wide abundance and excellent biocompatibility (Daniel and Astruc 2004; Sarma and Chattopodhyay 2004; Das et al. 2015; Chairam et al. 2009). However, majority of the starch-mediated synthesis reported are either chemical-based methods and/or produce AuNPs that are spherical or polyhedral in nature. Contrarily, use of starch as template material for synthesizing highly branched nanoparticles such as nanoflowers using plant extract as reducing agent has not been seen in the literature.

Results and discussion

Synthesis and characterization of gold nanoparticles

The gold nanoparticles are prepared by a simple in situ method using aqueous seed extract of the plant *Syzygium cumini* (L.) Skeels and HAuCl_4 . Formation of AuNPs was visually confirmed by observing the change in color from yellow to wine red. The UV–Vis spectra of the solution exhibited a strong surface plasmon resonance (SPR) band at 521 nm consistent with formation of AuNPs (supplementary Fig. S1) (Haiss et al. 2007). The formation of AuNPs was further confirmed by TEM analysis (Fig. 1a, b) and the spectra reveal that the NPs are well dispersed with both spherical and non-spherical morphologies with an average particle size of about 10 nm (Fig. 1c). Interestingly, when the same synthesis was carried out using starch (0.3% w/v) as additive, the SPR band showed a significant red shift. Instead of the peak at 521 nm, a broad peak at around 597 nm was observed (supplementary Fig. S1). Literature survey revealed that this type of broad peak usually observed for branched nanoparticles such as nanoflower (He et al. 2015; Xie et al. 2008). In fact, the HRTEM (Fig. 1g, h) and FESEM images (Fig. 2) confirm the flower-like morphology of starch-assisted AuNFs. The size of the nanoflowers varies from 30 to 110 nm with an average size of 55 nm. It is apparent from the FESEM image that the starch surface acts as a template to bind gold nanocrystals forming flower-like

Fig. 1 TEM images: in the absence of starch **a** highly dispersed gold nanoparticles (AuNPs), **b** magnified image, **c** particle size distribution. In the presence of 0.15% starch **d** AuNPs, **e** magnified image, **f** particle size distribution. In the presence of 0.3% starch **g** gold nanoflowers (AuNFs), **h** magnified image, **i** particle size distribution



aggregate. It is interesting to note that when the nanoparticle synthesis was carried out using starch at a lower concentration (0.15% w/v) (Fig. 1 d, e), no flower formation was observed and the TEM spectral patterns are almost similar to that of the starch-free AuNPs. Thus, it may be concluded that 0.3% (w/v) starch is essential to form the template for nanoflower synthesis.

The FTIR spectra of the starch-free AuNPs and starch-assisted AuNFs are shown in Supplementary Fig. S2. For comparison, the spectra of powdered seed sample are also presented. The seed powder shows prominent peaks at 3843, 3736, 3613, 1724 and 1521 cm^{-1} . The first three peaks are attributed to different types of polyphenolic –OH groups, while the peaks at 1724 and 1521 cm^{-1} are attributed to ν_{CO} and aromatic $\nu_{\text{C}=\text{C}}$ bands, respectively. Compared to the seed sample, the FTIR spectra of AuNPs and AuNFs show some prominent changes. For instance, the hydroxyl bands in the AuNFs appeared at 3869, 3739 and 3615 while in AuNPs appeared at 3763, 3683 and 3601 cm^{-1} . In a similar way, distinct shifts of carbonyl and C=C bands were also observed for AuNPs and AuNFs compared to the corresponding band of seed sample. Thus based on FTIR spectra, it could be concluded that in both the cases the Au nanoclusters are not

naked and are embedded with organic functionality present in the plant sample.

The XRD patterns of spectra of starch-free AuNPs and starch-assisted AuNFs are shown in Supplementary Fig. S3. Both the materials exhibited four prominent peaks with 2θ at around 38, 44, 64 and 78 corresponds to (111), (200), (220) and (311) planes, respectively (JCPDS no. 04-0784). The XPS survey spectra of AuNPs (supplementary Fig. S4) and AuNFs (supplementary Fig. S5) show that the nanomaterials contain carbon and oxygen with small amount of nitrogen and gold. Both the spectra are very similar. The binding energy peaks for C 1 s appears at around 284 eV and for O 1 s at around 532 eV corroborate with IR data that the nanomaterials contain carbonyl and hydroxyl groups. The Au 4f peak deconvoluted into two peaks of 4f7/2 and 4f5/2 with corresponding binding energies of 84.0 and 87.7 eV, respectively, consistent with metallic Au (supplementary Fig. S6). As expected, there is no significant difference observed in the XPS binding energy peaks of starch-free and starch-assisted Au nanoparticles.

The thermal stability of the starch-free AuNPs and starch-assisted AuNFs were analyzed by thermogravimetric analysis (TGA) and it was observed that the

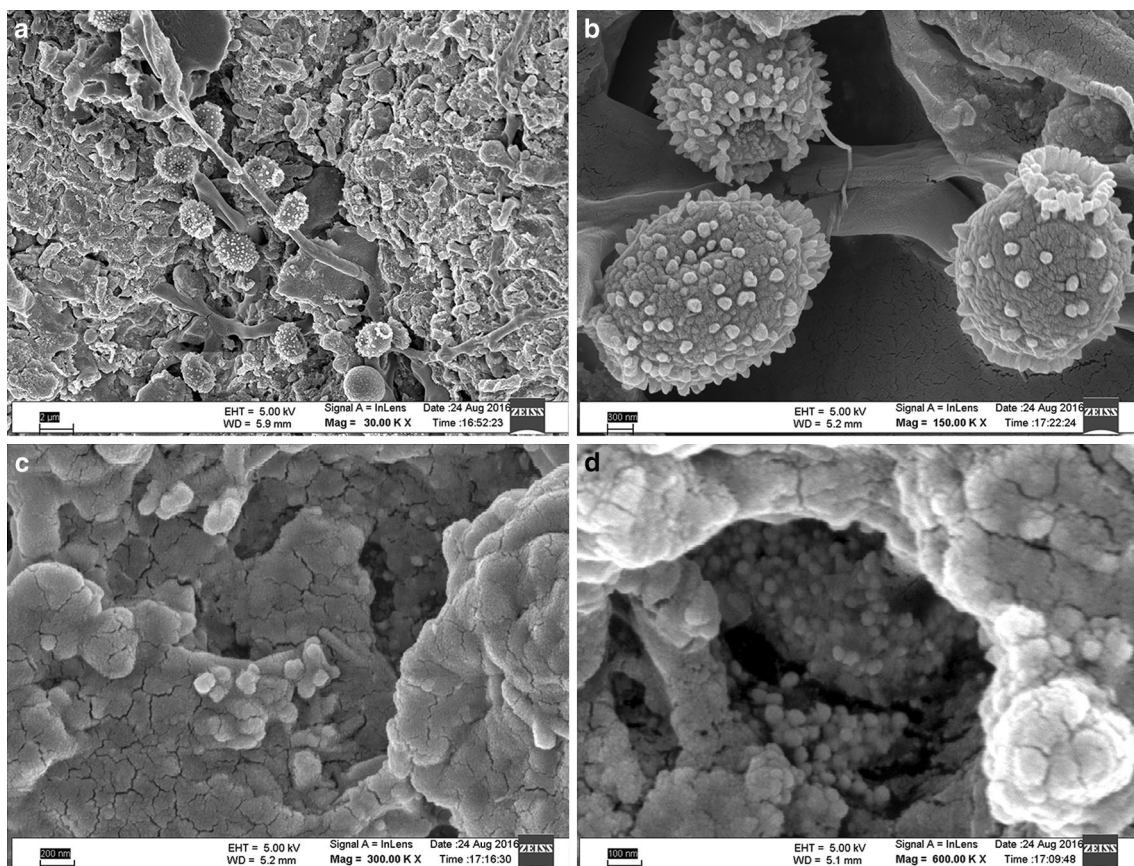


Fig. 2 FESEM images **a, b** starch-assisted AuNFs; **c, d** starch-free AuNFs

starch-assisted AuNFs was relatively more stable than the starch-free AuNFs (supplementary Fig. S7). The former one began to degrade at around 244 °C while the later one started degradation at around 226 °C. The TGA plot of the AuNFs showed an overall degradation of about 85% in two successive steps from 226 to 3600° C and from 360 to 6200° C. The first step was attributed to the phenolic –OH groups while the 2nd step was due to organic matter present in the seed extract. There was no decomposition observed after 621 °C, indicating that the remaining 14% was for metallic Au. The TGA spectra of AuNFs also showed a two-step thermal degradation but the spectral pattern is much different than that of the starch-free AuNFs. In the first step, a sharp weight loss of about 54% was observed between 244 and 345 °C, while in the 2nd step a gradual weight loss of about 30% occurs between 345 and 6800° C due to the bio-organic molecules present in the seed extract. In fact, the observed spectral pattern of AuNFs is very much similar to that of the free starch except the starch shows complete degradation, while AuNFs show 94% degradation and the residual 6% of no decomposition was due to metallic Au.

Antimicrobial assay

Due to the development of antibiotic resistance and the outbreak of infectious diseases caused by resistant pathogenic microbes, the researchers are now searching for new unconventional antimicrobial agents (Li et al. 2014). Literature survey reveals that gold nanoparticles synthesized through biological approach often demonstrate effective antimicrobial activity against different multi-drug-resistant (MDR) pathogens (Li et al. 2014; Annamalai et al. 2013). Hence, we have investigated the antimicrobial activity of both starch-free AuNFs and starch-assisted AuNFs against four bacterial strains that include one Gram positive (*Staphylococcus aureus* MTCC 121), two Gram negative (*Escherichia coli* MTCC 40 and *Pseudomonas aeruginosa* MTCC 4673) and one fungi (*Candida albicans* MTCC 227) by well diffusion method. Our results (Table S1) clearly indicate that among the four bacterial strains studied the best result was obtained against *E. coli* strain. Moreover, the diameter of zone of inhibition (Table S1) observed after incubation suggests starch-assisted flower-like nanoparticles are more effective than their starch-free counterparts against all the

strains under study. The superior performance of the AuNFs over simple AuNPs could be attributed to the better colloidal stability and larger surface area due to its multi-branched three-dimensional structure (Ji et al. 2015). Similar type of enhanced activities of flower-like gold nanoparticles over conventional AuNPs was also reported in literature for other biological applications (Ji et al. 2015 and; Xie et al. 2008). In fact, our control study showed that H₂AuCl₄ solution or plant extract alone does not show any antimicrobial activity (supplementary Table S1) against the MDR microbes under study. Although we did not study the antimicrobial effect using starch alone, it is expected that starch would not show any potential antimicrobial behavior against the MDR microbes as it is popularly used as an ingredient of various microbial growth media for its nutritional value (Vedder 1915). The AuNFs exerted an MIC of 0.06 mM for *C. albicans* (MTCC 227), *E. coli* (MTCC 40), and *S. aureus* (MTCC 121), and 0.08 mM against *P. aeruginosa* (MTCC 4673) (Fig. 3a–d) while the MBC values of 0.14 mM against all the strains except *E. coli*, against which the MBC value was found 0.12 mM only. Literature survey reveals that there exist a number of reports describing synthesis of AuNPs by plants such as *Abelmoschus esculentus* (Jayaseelan et al. 2013), *Euphorbia hirta* L. (Annamalai et al. 2013), *Brassica oleracea* (Piruthiviraj et al. 2016) that showed effective antimicrobial activity. However, a close study on the reported MIC/MBC values and/or the diameter of zone of inhibition suggests that the antimicrobial activity of our AuNFs is relatively superior compared to some of the reported values (Table 1, SI No 1–5).

Bacterial anti-efflux assay

The principle of the anti-efflux method was based on the ability of bacterial cells to expel EtBr, which is a pump substrate that allows the verification of the existence of an over-expressed efflux system relative to the intrinsic efflux activities of the corresponding wild-type strain. The presence of an efflux pump inhibitor (EPI) causes accumulation of EtBr in the cells and induces fluorescence at low concentration of EtBr (Christena et al. 2015). The anti-efflux activity of AuNPs was performed by cartwheel assay against all the microbial strains mentioned earlier by adding 0.005, 0.010 and 0.015 mM concentrations of Au NPs/Au NFs in nutrient agar media along with EtBr as a DNA intercalating dye to indicate the fluorescence released by the colony. The reference plates were devoid of Au NPs/Au NFs. When visualized under UV, significant increase in fluorescence of the test and control organism was observed indicating the inhibition of efflux activity of the strains (Fig. 4). Au NFs (Fig. 4b) showed better anti-efflux activity against all the microbial strains under study compared to that of Au NPs (Fig. 4a) in terms of fluorescence. Among the microbes under study *S. aureus* shows least fluorescence throughout. It has also been seen that the control in Fig. 4 shows some fluorescence behavior which could be due to the fact that some amount of EtBr (an intercalating dye used to detect fluorescence) remained entrapped inside the bacteria due to lesser expression of efflux activity. However, when gold nanoflowers are used, the fluorescence activity increases due to the blockage of efflux pump by the highly branched nanoparticles. Thus,

Fig. 3 Graph showing MIC and MBC results of Au NFs against different microbial strains at different time interval

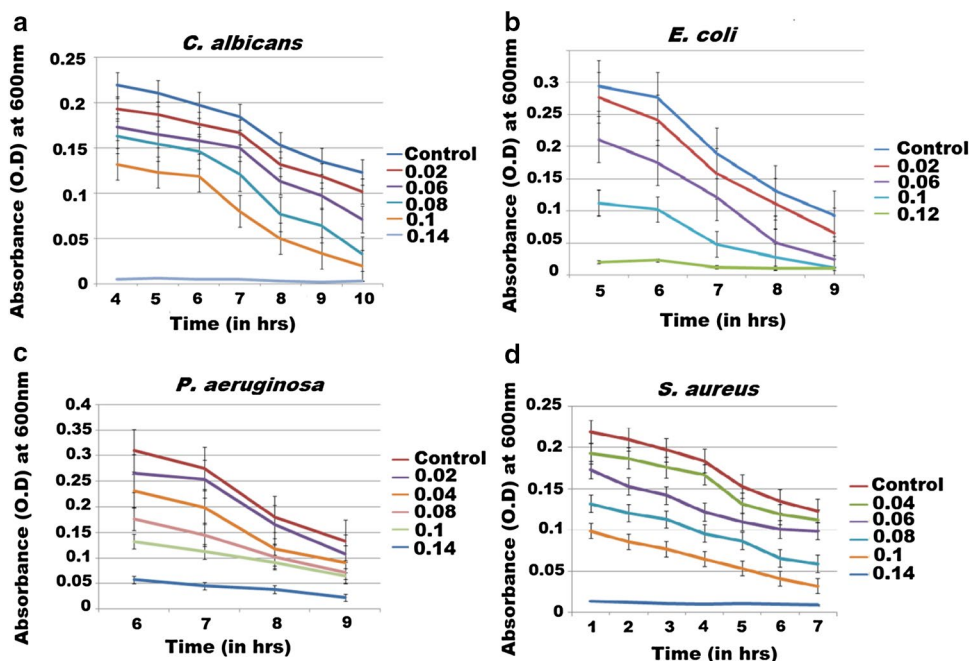


Table 1 Some recent reports on antimicrobial and anticancer studies by gold nanoparticles synthesized using plant extracts

Sl No.	Plant	Shape	Antimicrobial results			Anticancer results		References
			Experimental microbes	MIC	Zone of inhibition (mm)	Cell line used	Effective dose/IC ₅₀ value	
1	Leaf extract of carica papaya and <i>Cathartus roseus</i>	Spherical and polyhedral	<i>E. coli</i>	15.63 µg ml ⁻¹	20±0.7	Liver HepG2 and Breast MCF7 cell lines	> 150 µg ml ⁻¹	Muthukumar et al. (2016)
			<i>P. vulgaris</i>	62.5 µg ml ⁻¹	18±0.8			
			<i>S. aureus</i>	62.5 µg ml ⁻¹	–			
2	<i>Euphorbia hirta</i> L. leaf extract	Spherical	<i>B. subtilis</i>	1.25 µg ml ⁻¹	–	–	–	Annamalai et al. (2013)
			<i>E. coli</i>	1.25 µg ml ⁻¹	–			
3	<i>Abelmoschus esculentus</i>	Spherical	<i>P. aeruginosa</i>	–	17.0	–	–	Jayaseelan et al. 2013
			<i>K. pneumoniae</i>	–	18.0			
			<i>P. graminis</i>	–	16.0			
			<i>C. albicans</i>	–	15.0			
			<i>A. flavus</i>	–	20.0			
			<i>A. niger</i>	50 µg ml ⁻¹	9.0			
4	<i>Brassica oleracea</i>	Spherical	<i>A. flavus</i>	–	12.0	–	–	Piruthiviraj et al. (2016)
			<i>A. niger</i>	–	12.0			
			<i>C. albicans</i>	–	23.7			
			<i>E. coli</i>	0.06 mM	20.3			
5	<i>Syzygium cumini</i> (L.) skeels	Nanoflower	<i>P. aeruginosa</i>	0.08 mM	20.0	HepG2 cancer cell line	20 µg ml ⁻¹	Present study
			<i>C. albicans</i>	0.06 mM	20.0			
			<i>S. aureus</i>	0.06 mM	20.3			
6	<i>Pterocarpus marsupium</i>	Spherical and polyhedral	–	–	–	Breast (MDA-MB-231), cervical (HeLa), liver (Hep G2), lung (A549), pancreatic (MIA-Pa-Ca-2), and prostate (LN-CAP-FCG) cell lines	25 µg ml ⁻¹	Dhamecha et al. (2015)
			–	–	–			
7	<i>Mimosa pudica</i>	Spherical	–	–	Breast cancer cell lines (MDA-MB-231 & MCF-7)	10 µg ml ⁻¹	Suganya et al. (2016)	
8	<i>Genipa americana</i> fruit extract	Mostly spherical (15–40 nm)	–	–	Lung A-549 and cervical HeLa cells	–	Kumar et al. (2016)	
9	<i>Couroupita guianensis</i>	Spherical and polyhedral	–	–	Leukemia HL-60 cells	5.14–113.25 µM	Geetha et al. (2013)	
10	<i>Tabernaemontana divaricata</i> flower	Nearly spherical	–	–	MCF-7 cell line	100 µg ml ⁻¹	Preetam et al. (2016)	

Table 1 (continued)

Sl No.	Plant	Shape	Antimicrobial results		Anticancer results		References
			Experimental microbes	MIC	Cell line used	Effective dose/IC ₅₀ value	
11	<i>Sargassum glaucescens</i>	Spherical	–	–	Cervical (HeLa), liver (HepG2), breast (MDA-MB-231) and leukemia (CEM-ss) cell lines	4.75 µg ml ⁻¹ 7.14 µg ml ⁻¹ 10.32 µg ml ⁻¹ 11.82 µg ml ⁻¹	Ajdari et al. 2016

more amount of EtBr is expected to be accumulated by the bacteria.

Anti-biofilm activity

Biofilm plays a fundamental role in infectious diseases, as they form a biopolymer surface which resists antimicrobial agents. Biofilms are highly recalcitrant and because of their heterogeneity and slow growth phenotypes and hence the antimicrobial agents that are potent against planktonic cells may not be effective against the biofilm mode of growth. The Au NFs exhibited their potential as biofilm inhibitor against all the bacterial strains irrespective of Gram-positive and -negative cell wall as well as against the fungal strain under the study. Anti-biofilm assay against *C. albicans*, *E. coli*, *P. aeruginosa* and *S. aureus* was investigated in-vitro by monitoring the binding of the dye crystal violet to adherent cells, which directly revealed their effective ability in formation of biofilm (Merritt et al. 2005; O'Toole 2011). Maximum inhibition of biofilm was recorded at 0.5 mM concentration of Au NFs (Fig. 5a). It showed 74, 71, 59, and 55% of biofilm disruption against *S. aureus*, *C. albicans*, *P. aeruginosa*, and *E. coli*, respectively (Fig. 5b). However, significant decrease ($\geq 50\%$ inhibition) in biomass formation was also observed at 0.45, 0.4 and 0.25 mM concentrations of Au NFs. It was further validated by monitoring the decrease in protein and EPS (exo-polysaccharides) level in the EPS layer secreted by respective organism (supplementary Fig. S8). The subsequent decrease in the biofilm components (i.e., EPS and protein) of all the experimental microbes after treating with AuNFs confirms efficient detachment of biofilms. The present study reports significant reduction of biofilm formation at a concentration as low as 0.26 mM Au NFs. It may be noted from Fig. S8 that even though visual observation of the graph shows no significant difference between AuNP and AuNF, the difference in the results is statistically significant ($p < 0.05$) as they were performed in triplicates and is expressed in Mean \pm SD.

In-vitro cytotoxicity assay

The cytotoxicity assay of AuNFs was carried out on sheep erythrocytes keeping in mind the fact that all drugs finally reach blood stream after metabolism. The ability of nanoparticles to induce apoptosis (programmed cell death) was assessed using Cy3-Annexin V staining. Fluorescence microscopy was used to monitor the fluorescence released from apoptotic cell and the images are displayed in supplementary Fig. S9. For comparison, tap water was used as positive control (S9a). Trypan blue dye exclusion technique was used to determine cell viability. It is clearly visible from the figures that the control (Fig. S9a) is showing more fluorescence compared to the test samples, i.e. AuNFs (Fig.

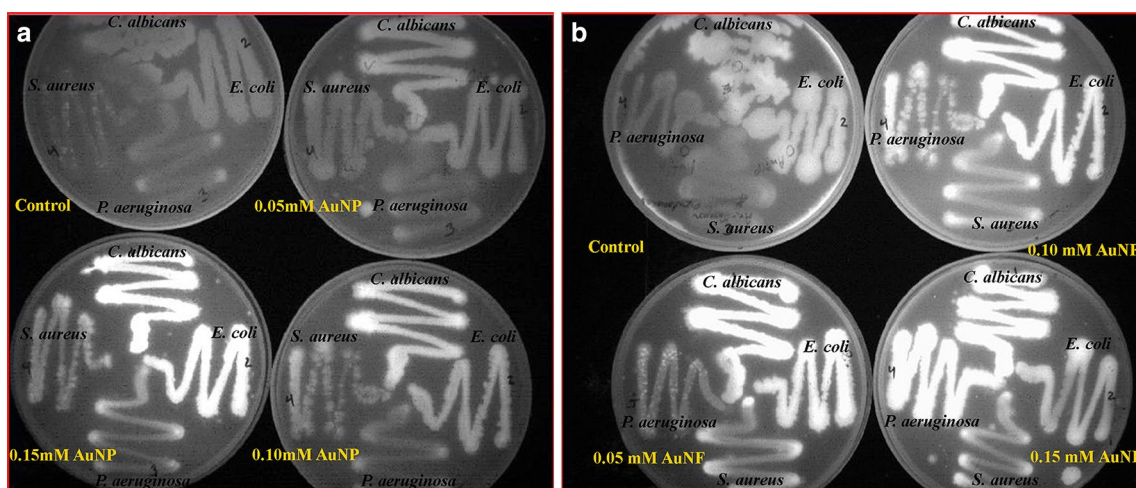


Fig. 4 Comparative efflux activity in terms of fluorescence released by the microbial colonies at different concentration of **a** Au NPs and **b** Au NFs

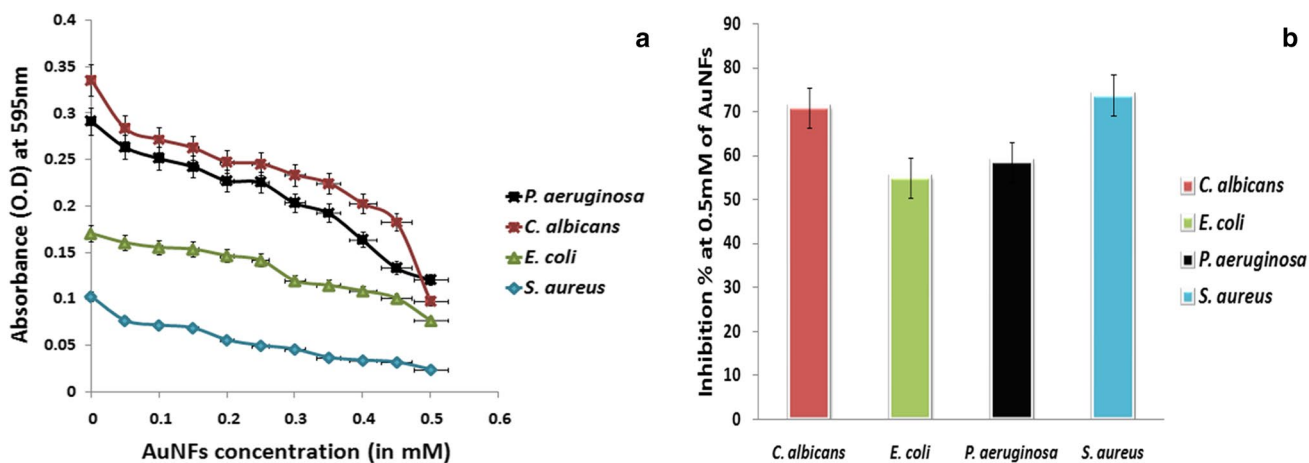


Fig. 5 **a** Graph showing inhibition of biofilm formation with gradual increase in AuNFs concentration in the media; **b** comparative inhibition of biofilm with highest concentration of Au NFs (0.5 mM) against different microbial strains

S9b), which indicate more number of cell deaths in the case of control compared to test. Our study shows that almost 99% of RBCs display healthy status at a concentration of $20 \mu\text{g mL}^{-1}$ of AuNFs while tap water shows 54%.

In-vitro anticancer assay

Cancer is one of the major diseases that cause maximum numbers of death around the world and hence considerable efforts are being made to develop novel anticancer drugs. Over the past few years, nanoparticle-based cancer medicine has received immense popularity because of their targeted delivery. Among various metal nanoparticles, nanogold is

particularly promising for their easy synthesis, chemical inertness, biocompatibility, and low level of cytotoxicity (Dreaden et al. 2011). Thus, we are intrigued to see the effectivity of the AuNFs for anticancer activity. Human liver cancer cell line HepG2 was chosen for our study. The in-vitro anticancer activity of AuNFs was carried out by MTT assay. We are gratified to see that the AuNFs effectively inhibited the proliferation of HepG2 cell. The IC_{50} value of the AuNFs was found to be $20 \mu\text{g mL}^{-1}$ which is about four times higher than that of the standard anticancer drug, cyclophosphamide monohydrate ($\text{IC}_{50} = 4 \mu\text{g mL}^{-1}$). The above-mentioned concentration of AuNFs was not found to be cytotoxic against normal sheep erythrocytes. Although

the IC_{50} of the AuNFs is higher compared to the standard drug, our result is quite significant as the production of AuNFs is expected to be more cost effective and biocompatible compared to the production of cyclophosphamide monohydrate. The microscopic photographs of normal and treated cancer cells of HepG2 are shown in Fig. 6. It is worth noting here that there are a few reports available (Table 1) where gold nanoparticles synthesized using plant extracts as reducing agents showed promising in vitro anticancer activities against various kinds of cancers such as breast, cervical, liver, lung, prostate, and leukemia; however the effectiveness of such systems depends on various factors that includes size and shapes of the NPs, types of cancers, nature of biogenic sources, etc. For instance, recently Dhamecha et al. 2015 (Table 1, Sl. No. 6) reported synthesis of AuNPs using *Pterocarpus marsupium* that showed excellent anticancer activities against breast, lung and prostate, while relatively poor activities were observed with cervical or liver cell lines. In another example, Preetam Raj et al. 2016 reported synthesis of AuNPs by aqueous flower extract of *T. divaricata* that showed effective anticancer activity against breast cancer cell line MCF-7 with IC_{50} value of $100 \mu\text{g mL}^{-1}$ (Table 1, Sl. No.10).

Conclusions

In conclusion, we described a morphology-controlled synthesis of gold nanoparticles using aqueous seed extract of *Syzygium cumini* (L.) as bio-reductant. Gold nanoparticles with flower-like morphology are obtained when the synthesis was carried out in the presence of starch (0.3%), while in the absence of starch only quasi-spherical or polyhedral nanoparticles are formed. The gold nanoparticles function as effective antimicrobial and anti-biofilm agents against four bacterial strains. Control experiments revealed that the flower-like nanoparticles are more effective than the

polyhedral nanoparticles. The AuNFs also showed effective in vitro anticancer activity against liver cancer HepG2 cell line with no significant cytotoxicity.

Materials and methods

Chloroauric acid (HAuCl_4) was purchased from Merck India Pvt. Ltd. All the bacteriological media used in the present study were procured from HiMedia Laboratories Pvt. Ltd. The other common laboratory chemicals are of analytical grade and were purchased from different Indian firms. The FTIR spectra ($4000\text{--}400 \text{ cm}^{-1}$) were recorded in KBr on a Shimadzu IR prestige-21 spectrophotometer. X-ray diffraction (XRD) study was performed in a Rigaku diffractometer (model: ULTIMA IV) with a $\text{Cu K}\alpha$ source ($\lambda = 1.54056 \text{ \AA}$) from 5° to 100° . The TEM analysis was carried out on a JEOL JEM-2011 electron microscope operated at an accelerating voltage of 200 kV. XPS study was performed at “Centro de Materiais da Universidade do Porto” (Portugal), using a Kratos Axis Ultra HSA spectrometer with a non-monochromatized $\text{Mg K}\alpha$ radiation (1253.6 eV). FESEM analysis was performed using ZEISS, SIGMA instrument. Thermogravimetric analyses were done using PerkinElmer STA 8000 from temperature range 50 to 750°C at the heating rate of $10^\circ\text{C min}^{-1}$ at 30 mL min^{-1} nitrogen flow rate. Bacterial growth was measured with the help of UV–Vis spectrophotometer (Shimadzu UV-1800, Japan).

Preparation of seed extract

10 g of powdered *S. cumini* (L.) Skeel seeds was mixed in 1000 mL of deionized water and then boiled for 30 min. The resultant mixture was then cooled and filtered through Whatman No. 1 filter paper. The filtrate was considered as seed extract and stored at room temperature until further use.

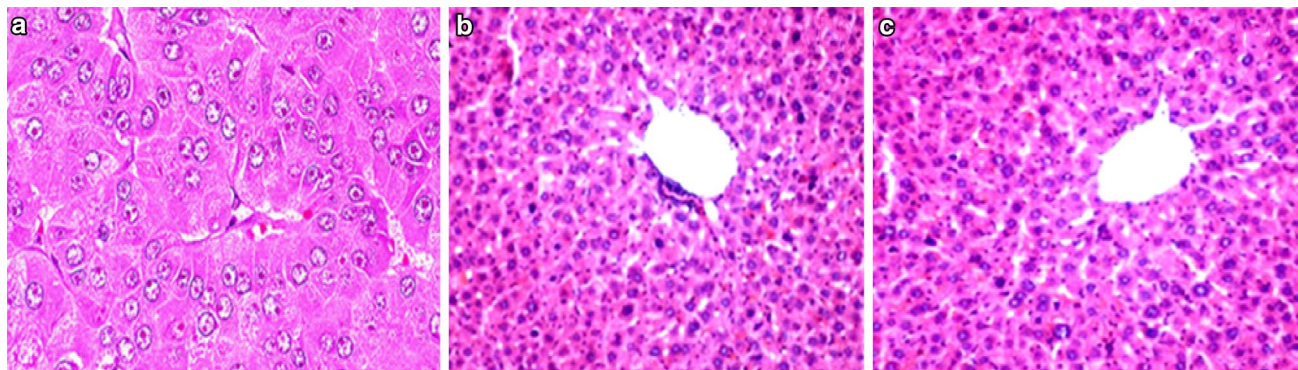


Fig. 6 Microscopic images of liver cancer cell line HepG2: **a** normal cancer cell before treatment, **b** after treatment with $4 \mu\text{g mL}^{-1}$ cyclophosphamide monohydrate, and **c** after treatment with $20 \mu\text{g mL}^{-1}$ AuNFs

Synthesis of gold nanoparticles (AuNPs)

500 mL of aqueous HAuCl_4 (1 mM) was added to 1000 mL of the seed extract under stirring condition. The mixture was stirred for 1 h at room temperature and during that time the color of the solution changed from yellow to wine red confirming reduction of Au^{3+} to Au^0 . To ensure complete reduction, the resultant mixture was further autoclaved at 15 psi pressure at 121 °C for 15 min. After cooling the reaction mixture to room temperature, the resultant nanoparticles were obtained through centrifugation at 4 °C for 15 min.

Synthesis of flower-like gold nanoparticles (AuNFs)

The flower-like nanoparticles are synthesized by adding 0.3% (w/v) of soluble starch to the seed extract. All other conditions are same as mentioned in the synthesis of AuNPs, except color of the solution changed from yellow to blue.

Determination of antimicrobial properties

Agar well diffusion assay

Overnight microbial cultures (10^7 – 10^8 cfu mL^{-1}) of *S. aureus* (MTCC 121), *E. coli* (MTCC 40), *P. aeruginosa* (MTCC 4673), and *C. albicans* (MTCC 227) were inoculated by spread plating method on Mueller–Hinton (MH) agar plates. Antimicrobial activities of AuNPs/AuNFs against these strains were evaluated by agar well diffusion method by loading 100 μL of AuNPs/AuNFs (0.15 mM), HAuCl_4 sol (1 mM) and plant extract separately in respective wells of the microbial plates followed by 24 h of incubation at 37 °C. Antimicrobial effect was confirmed by observing the zone of inhibition around the well.

Determination of MIC and MBC

MIC and MBC of AuNPs/AuNFs were determined using standard broth dilution method. Briefly, sterile test tubes each containing 1 mL of LB (Luria Bertani) broth were inoculated with 10 μL of freshly prepared each of the microbial suspensions taken in individual tubes to maintain initial microbial concentration 10^3 – 10^4 cfu mL^{-1} . To these, the AuNPs was added in such a way that it gives 0.02, 0.04, ... 0.14 mM final concentration in 1 mL of overnight microbial broth. Bacterial growth was measured as an increase or decrease in the absorbance at 600 nm by UV–Vis spectrophotometer at an interval of 1 h after incubation.

Evaluation of microbial anti-efflux activity

To evaluate the bacterial anti-efflux activity, ethidium bromide was added at a concentration of 0.5 $\mu\text{g mL}^{-1}$ to the

nutrient agar plates supplemented with AuNPs/AuNFs at different concentrations (0.005, 0.010 and 0.015 mM). The control plate was set without adding NPs. Microbial strains were then inoculated on the plates by streak plating method. The NPs (AuNPs/AuNFs) giving better anti-efflux activities based on fluorescence released was considered for further studies.

Anti-biofilm assay

Destruction of microbial biofilm was evaluated using crystal violet staining method. Briefly, 100 μL of the most potential nanomaterials with the concentrations ranging from 0.05, 0.1, ... to 0.5 mM were taken in separate wells of a polystyrene 96-well plate. To these, 100 μL of (1:100) overnight microbial cultures dilutions with fresh LB broth was added. Control was set without nanomaterial. After 24 h of incubation at 37 °C, the plates were washed twice with phosphate buffered saline (PBS) to remove the unbound cells and left for air-drying. The plates were then stained with 0.1% crystal violet (250 μL) and the excess stain was removed by washing with PBS. The nanomaterial-treated biofilm was quantified by extracting crystal violet stain using 30% acetic acid and taking absorbance at 595 nm using 30% acetic acid in water as a blank. Protein and exo-polysaccharide (EPS) content in the treated biofilms was further estimated (Nithyanand et al. 2010). The collected suspension was used as source for studying biochemical composition in terms of total protein determined by Lowry et al. 1951 and total carbohydrate by Anthrone method (Loewus 1952).

Cytotoxicity assay

Cytotoxicity assay was done by fluorescence microscopy using AnnexinV staining kit. A total volume of 0.8 mL for each dilution of AuNFs (1, 2, 3, ..., 40 $\mu\text{g mL}^{-1}$ in phosphate buffer saline) was taken in separate Eppendorf. Fresh sheep erythrocytes (5×10^5 RBCs mL^{-1}) were added to each tube to give a final volume of 1 mL and incubated at 37 °C for 1 h followed by centrifugation at 6000 rpm for 5 min. A negative control tube (containing PBS only) and a positive control tube (containing tap water) were also included in the analysis. Further, RBCs were resuspended in 500 μL binding buffer and then stained with 5 μL AnnexinV stain for 5 min followed by visual examination by fluorescence microscope. Viability of the cells was determined by transferring 50 μL of RBC suspension mixed in equal volume of trypan blue stain to a haemocytometer. The number of cells per mL and viable cell percentage was calculated using the following formula (Wilson 2000):

$$\text{Total } \frac{\text{cells}}{\text{mL}} = \frac{\text{Total cells counted} \times \text{Dilution factor}}{\text{No. of squares in haemocytometer}} \times 10,000 \text{ cells,}$$

$$\% \text{ Viability of cells} = \frac{\text{Live cell count}}{\text{Total cell count}} \times 100.$$

In-vitro anticancer assay

In-vitro anticancer assay on liver cancer cell line HepG2 was done by MTT (5-diphenyl tetrazolium bromide) assay. The monolayer of HepG2 cell line was trypsinized and the cell count was adjusted to 3×10^5 cells mL^{-1} using medium containing 10% newborn calf serum. 100 μL of this suspension was loaded in each well of 96-well microtitre plates. The supernatant was flicked off after incubation and 100 μL of different concentrations of AuNPs (10, 20, ..., 100 $\mu\text{g mL}^{-1}$) were added to the cells in each well and kept for incubation at 37 °C in 5% CO_2 incubator for 72 h. After incubation, the solution in wells was drained off and 50 μL of MTT dye was added to each well. The supernatant was removed and 50 μL of propanol was added. The absorbance was measured using a microplate reader at a wavelength of 490 nm (Wilson 2000; Riss et al. 2004). Microscopic examination was done by treating 50 μL of cells with equal volume of trypan blue stain.

Statistical analysis

Each experiment was performed in triplicates and results are expressed in terms of standard deviation (SD) \pm mean. Students' *t*-test was performed by Graphpad software (<http://www.graphpad.com>) to see the significance of *p* value obtained, and is greater than the 0.05 probability value.

Acknowledgements The Department of Biotechnology, New Delhi, is gratefully acknowledged for financial support (Grant No. MED/2013/23) and also for Delcon E-journals facility to Dibrugarh University. The UGC, New Delhi, has also been acknowledged for the SAP-DRS-I grant to the Department of Chemistry. The service of SAIF, NEHU, Shillong, was gratefully acknowledged for TEM analysis. The authors specially acknowledge Dr. Abhishek Mathur, National Center for Fungal Taxonomy, New Delhi, for cytotoxicity and anticancer study.

References

- Ackerson CJ, Jadzinsky PD, Jensen GJ, Kornberg RD (2006) Rigid, specific, and discrete gold nanoparticle/antibody conjugates. *J Am Chem Soc* 128:2635–2640
- Ahn S, Singh P, Jang M, Kim Y-J, Castro-Aceituno V, Simu SY, Kim YJY, Yang D-C (2017) Gold nanoflowers synthesized using *acanthopanax* cortex extract inhibit inflammatory mediators in LPS-induced RAW264.7 macrophages via NF- κ B and AP-1 pathways. *Colloids Surf B Biointerfaces*. <https://doi.org/10.1016/j.colsurfb.2017.11.037>
- Ajdari Z, Rahman H, Shameli K, Abdullah R, Ghani MA, Yeap S, Abbasiliasi S, Ajdari D, Ariff A (2016) Novel gold nanoparticles reduced by *sargassum glaucescens*: preparation, characterization and anticancer activity. *Molecules* 123:1–17

- Annamalai A, Christina VLP, Sudha D, Kalpana M, Lakshmi PTV (2013) Green synthesis, characterization and antimicrobial activity of Au NPs using *Euphorbia hirta L.* leaf extract. *Colloids Surf B Biointerfaces* 108:60–65
- Astruc D (2007) Nanoparticles and catalysis. Wiley-VCH Verlag GmbH & Co. KGaA, Weinheim
- Bakr OM, Wunsch BM, Stellacci F (2006) High-yield synthesis of multi-branched urchin-like gold nanoparticles. *Chem Mater* 18:3297–3301
- Chairam S, Poolperm C, Somsook E (2009) Starch vermicelli template-assisted synthesis of size/shape-controlled nanoparticles. *Carbohydr Polym* 75:694–704
- Christena LR, Mangalagowri V, Pradheeba P, Ahmed KBA, Shalini BIS, Vidyalakshmi M, Anbazhagan V, Subramanian NS (2015) Copper nanoparticles as an efflux pump inhibitor to tackle drug resistant bacteria. *RSC Adv* 5:12899–12909
- Costa NJ, Rossi LM (2012) Synthesis of supported metal nanoparticle catalysts using ligand assisted methods. *Nanoscale* 4:5826–5834
- Daniel M-C, Astruc D (2004) Gold nanoparticles: assembly, supramolecular chemistry, quantum-size-related properties, and applications toward biology, catalysis, and nanotechnology. *Chem Rev* 104:293–346
- Das RK, Borthakur BB, Bora U (2010) Green synthesis of gold nanoparticles using ethanolic leaf extract of *Centella asiatica*. *Mater Lett* 64:1445–1447
- Das S, Pandey A, Pal S, Kolya H, Tripathy T (2015) Green synthesis, characterization and antibacterial activity of gold nanoparticles using hydroxyethyl starch-*g*-poly (methylacrylate-*co*-sodium acrylate): a novel biodegradable graft copolymer. *J Mol Liq* 212:259–265
- Das P, Chetia B, Prasanth R, Jagan Madhavan J, Singaravelu G, Benelli G, Murugan K (2017) Green nanosynthesis and functionalization of gold nanoparticles as PTP 1B inhibitors. *J Clust Sci* 28:2269–2277
- Dauthal P, Mukhopadhyay M (2016) Noble metal nanoparticles: plant-mediated synthesis, mechanistic aspects of synthesis, and applications. *Ind Eng Chem Res* 55:9557–9577
- Dhamecha D, Jalalpure S, Jadhav K (2015) Doxorubicin functionalized gold nanoparticles: characterization and activity against human cancer cell lines. *Process Biochem* 50:2298–2306
- Dreaden EC, Mackey MA, Huang X, Kang B, El-Sayed MA (2011) Beating cancer in multiple ways using nanogold. *Chem Soc Rev* 40:3391–3404
- Geetha R, Ashokkumar T, Tamilselvan S, Govindaraju K, Sadiq M, Singaravelu G (2013) Green synthesis of gold nanoparticles and their anticancer activity. *Cancer Nano* 4:91–98
- Giljohann DA, Seferos DS, Daniel WL, Massich MD, Patel PC, Mirkin CA (2010) Gold Nanoparticles for biology and medicine. *Angew Chem Int Ed* 49:3280–3294
- Grzelczak M, Pe'rez-Juste J, Mulvaney P, Liz-Marzán LM (2008) Shape control in gold nanoparticle synthesis. *Chem Soc Rev* 37:1783–1791
- Gupta RK, Krishnamoorthy S, Kusuma DY, Lee PS (2012) Enhancing charge-storage capacity of non-volatile memory devices using template-directed assembly of gold nanoparticles. *Nanoscale* 4:2296–2300
- Haiss W, Thanh NTK, Aveyard J, Fernig DG (2007) Determination of size and concentration of gold nanoparticles from UV-Vis spectra. *Anal Chem* 79:4215–4221
- He Y, Zang S, Liu Y, He Y, Lei H (2015) A multi-walled carbon nanotubes-poly(L-lysine)modified en-antioselective immunosensor for ofloxacin by using multi-enzyme-la-beled gold nanoflower as signal enhancer. *Biosens Bioelectron* 73:85–92
- Jana NR, Gearheart L, Murphy CJ (2001) Seeding growth for size control of 5–40 nm. Diameter Gold Nanoparticles *Langmuir* 17:6782–6786

- Jayaseelan C, Ramkumar R, Rahuman AA, Peruma P (2013) Green synthesis of gold nanoparticles using seed aqueous extract of *Abelmoschus esculentus* and its antifungal activity. *Ind Crops Prod* 45:423–429
- Ji Y, Ren M, Li Y, Huang Z, Shu M, Yang H, Xiong Y, Xu Y (2015) Detection of aflatoxin B1 with immunochromatographic test strips: enhanced signal sensitivity using gold nanoflowers. *Talanta* 142:206–212
- Kumar V, Yadav SK (2012) Characterisation of gold nanoparticles synthesised by leaf and seed extract of *Syzygium cumini* L. *J Exp Nanosci* 7:440–451
- Kumar B, Smita K, Cumbal L, Camacho J, Hernández-Gallegos E, Chávez-López MG, Grijalva M, Andrade K (2016) One pot phytosynthesis of gold nanoparticles using *Genipa americana* fruit extract and its biological applications. *Mater Sci Eng C* 62:725–731
- Langille MR, Personick ML, Zhang J, Mirkin CA (2012) Defining rules for the shape evolution of gold nanoparticles. *J Am Chem Soc* 134:14542–14554
- Li Y, Wu T-Y, Chen S-M, Ali MA, AlHemaid FM (2012) Green synthesis and electrochemical characterizations of gold nanoparticles using leaf extract of *Magnolia kobus*. *Int J Electrochem Sci* 7:12742–12751
- Li X, Robinson SM, Gupta A, Saha K, Jiang Z, Moyano DF, Sahar A, Riley MA, Rotello VM (2014) Functional gold nanoparticles as potent antimicrobial agents against multi-drug-resistant bacteria. *ACS Nano* 8:10682–10686
- Liu X, Xu H, Xia H, Wang D (2012) Rapid seeded growth of monodisperse, quasi-spherical, citrate-stabilized gold nanoparticles via H₂O₂ reduction. *Langmuir* 28:13720–13726
- Liu F, Liu C, Liu W, Ding Z, Ma H, Seeram NP, Xu L, Yu Mu Y, Huang X, Li L (2017) New sesquiterpenoids from *Eugenia jambolana* seeds and their anti-microbial activities. *J Agric Food Chem* 65:10214–10222
- Loewus FA (1952) Improvement in anthrone method for determination of carbohydrates. *Anal Chem* 24:219–219
- Lowry OH, Rosebrough NJ, Farr AL, Randall RJ (1951) Protein measurement with the folin phenol reagent. *J Biol Chem* 193:265–275
- Mao K, Chen Y, Wu Z, Zhou X, Shen A, Hu J (2014) Catalytic strategy for efficient degradation of nitroaromatic pesticides by using gold nanoflower. *J Agri Food Chem* 62:10638–10645
- Mata R, Bhaskaran A, Sadras SR (2016) Green-synthesized gold nanoparticles from *Plumeria alba* flower extract to augment catalytic degradation of organic dyes and inhibit bacterial growth. *Particulology* 24:78–86
- Merritt JH, Kadouri DE, O'Toole GA (2005) Growing and analyzing static biofilms. *Curr Protoc Microbiol*. <https://doi.org/10.1002/9780471729259.mc01b01s00>
- Misra M, Singh N, Gupta RK (2017) Enhanced visible-light-driven photocatalytic activity of Au@Ag core-shell bimetallic nanoparticles immobilized on electrospun TiO₂ nanofibers for degradation of organic compounds. *Catal Sci Technol* 7:570–580
- Mohanty A, Garg N, Jin RA (2010) A Universal approach to the synthesis of noble metal nanodendrites and their catalytic properties. *Angew Chem Int Ed* 49:4962–4966
- Muthukumar T, Sambandam B, Aravinthand A, Sastrya TP, Kim J-H (2016) Green synthesis of gold nanoparticles and their enhanced synergistic antitumor activity using HepG2 and MCF7 cells and its antibacterial effects. *Process Biochem* 51:384–391
- Nanoparticles with Tunable Longitudinal Plasmon Resonance. *Langmuir* 20: 3520–3524
- Nithyanand P, Thenmozhi R, Rathna J, Pandian SK (2010) Inhibition of *Streptococcus pyogenes* biofilm formation by coral-associated actinomycetes. *Curr Microbiol* 60:454–460
- O'Toole GA (2011) Microtiter Dish Biofilm Formation Assay. *J Vis Exp* 47:e2437
- Opris R, Tatomir C, Olteanu D, Moldovan R, Moldovan B, David L, Nagy A, Decea N, Kiss ML, Filip GA (2017) The effect of *Sambucus nigra* L. extract and phytosynthesized gold nanoparticles on diabetic rats. *Colloids Surf B Biointerfaces* 150:192–200
- Personick ML, Mirkin CA (2013) Making sense of the mayhem behind shape control in the synthesis of gold nanoparticles. *J Am Chem Soc* 135:18238–18247
- Phukan S, Bharali P, Das AK, Rashid MH (2016) Phytochemical assisted synthesis of size and shape tunable gold nanoparticles and assessment of their catalytic activities. *RSC Adv* 6:49307–49316
- Piruthiviraj P, Margret A, Krishnamurthy PP (2016) Gold nanoparticles synthesized by *Brassica oleracea* (Broccoli) acting as antimicrobial agents against human pathogenic bacteria and fungi. *Appl Nanosci* 6:467–473
- Preetam Raj JP, Purushothaman M, Khusro A, Panicker SG (2016) In-vitro anticancer and antioxidant activity of gold nanoparticles conjugate with *Tabernaemontana divaricata* flower SMS against MCF-7 breast cancer cells. *Korean Chem Eng Res* 54:75–80
- Riss TL, Moravec RA, Niles AL, Duellman MSS, Benink HA, Worzella TJ, Minor L (2004) Cell Viability Assays. Eli Lilly & Company and the National Center for Advancing Translational Sciences
- Sarma TK, Chattopodhyay A (2004) Starch-mediated shape-selective synthesis of Au nanoparticles with tunable longitudinal plasmon resonance. *Langmuir* 20:3520–3524
- Schreiber R, Santiago I, Ardavan A, Turberfield AJ (2016) Ordering gold nanoparticles with DNA origami nanoflowers. *ACS Nano* 10:7303–7306
- Siddiqi KS, Husen A (2017) Recent advances in plant-mediated engineered gold nanoparticles and their application in biological system. *J Trace Elem Med Biol* 40:10–23
- Singh N, Gupta RK, Lee PS (2011) Gold-nanoparticle-functionalized In₂O₃ nanowires as CO gas sensors with a significant enhancement in response. *ACS Appl Mater Interfaces* 3:2246–2252
- Soetan N, Zarick HF, Banks C, Webb JA, Libson G, Coppola A, Bardhan R (2016) Morphology-directed catalysis with branched gold nanoantennas. *J Phy Chem C* 120:10320–10327
- Suganya KSU, Govindaraju K, Kumar VG, Prabhu D, Arulvasu C, Dhas TS, Karthick V, Changmai N (2016) Anti-proliferative effect of biogenic gold nanoparticles against breastcancer cell lines (MDA-MB-231 & MCF-7). *Appl Surf Sci* 371:415–424
- Swami SB, Thakor NSJ, Patil MM, Haldankar PM (2012) Jamun (*Syzygium cumini* (L.)): a review of its food and medicinal uses. *Food Nut Sc* 3:1100–1117
- Tiwari AD, Mishra AK, Mishra SB, Arotiba OA, Mamba BB (2011) Green synthesis and stabilization of gold nanoparticles in chemically modified chitosan matrices. *Int J Biol Macromol* 48:682–687
- Virkutyte J, Varma RS (2011) Green synthesis of metal nanoparticles: Biodegradable polymers and enzymes in stabilization and surface functionalization. *Chem Sci* 2:837–846
- Wang Z, Zhang J, Ekman JM, Kenis PJA, Lu Y (2010) DNA-mediated control of metal nanoparticle shape: one-pot synthesis and cellular uptake of highly stable and functional gold nanoflowers. *Nano Lett* 10:1886–1891
- Wilson P (2000) Cytotoxicity and viability assays in animal cell culture: a practical approach. Masters J. R.W. (ed) Oxford: Oxford University Press
- Xiao J, Qi L (2011) Surfactant-assisted, shape-controlled synthesis of gold nanocrystals. *Nanoscale* 3:1383–1396
- Xie J, Zhang Q, Lee JY, Wang DIC (2008) The synthesis of SERS-Active gold nanoflower tags for in vivo applications. *ACS Nano* 2:2473–2480
- Yang X, Yang M, Pang B, Vara M, Xia Y (2015) Gold nanomaterials at work in biomedicine. *Chem Rev* 115:10410–10488
- Ye S, Benz F, Wheeler MC, Oram J, Baumberg JJ, Cespedes O, Christenson HK, Coletta PL, Jeuken LJC, Markham AF, Critchleya K,

- Evans SD (2016) One-step fabrication of hollow-channel gold nanoflowers with excellent catalytic performance and large single-particle SERS activity. *Nanoscale* 8:14932–14942
- Zhao L, Ji X, Sun X, Li J, Yang W, Peng X (2009) Formation and stability of gold nanoflowers by the seeding approach: the effect of intraparticle ripening. *J Phys Chem C* 113:16645–16651
- Zhu M, Lanni E, Garg N, Bier ME, Jin R (2008) Kinetically controlled, high-yield synthesis of Au₂₅ clusters. *J Am Chem Soc* 130:1138–1139

Publisher's Note Springer Nature remains neutral with regard to jurisdictional claims in published maps and institutional affiliations.